Back to Session Subjects

THE ORTHOGONAL BLADE-VORTEX INTERACTION EXPERIMENTAL PROGRAMME AT THE UNIVERSITY OF GLASGOW

C.J. Doolan, R.B. Green, F.N. Coton and R.A.McD. Galbraith

Department of Aerospace Engineering, University of Glasgow

Glasgow, Scotland, UK

Abstract

Research into blade-vortex interactions (BVI) has been undertaken at the University of Glasgow for a number of years. In the past, these investigations have concentrated on main-rotor BVI. More recently, however, the focus of the research has turned to main rotor/tail rotor BVI where one possible interaction geometry is the orthogonal interaction. The present paper describes an experimental programme aimed at investigating this particular phenomenon. Although not complete, the research has already identified several key features of the orthogonal interaction including the significance of the axial flow component within the trailed tip vortex. It has also isolated the effect of blade incidence and vortex pre-cut. These characteristics will be described and discussed in the paper. Finally, the remaining elements of the research programme will also be outlined.

Nomenclature

C_n	normal force coefficient, [**N**/($1/2\rho V_\infty^2$ c)]
C_m	1/4 chord pitching moment coefficient, [M/($1/2\rho V_\infty^2$ c^2)]
Cp	pressure coefficient, [$(p-p_\infty)$/($1/2\rho V_\infty^2$)]
c	interacting blade chord, (m)
c_R	rotor blade chord, (m)
N	normal force per unit span, (Nm^{-1})
M	1/4 chord pitching moment per unit span, (N)
R	rotor radius, (m)
r_c	vortex core radius, (m)
t	time, (s)
u	streamwise velocity component, (ms^{-1})
V_∞	freestream velocity, (ms^{-1})
v	vertical velocity, (ms^{-1})
W	vortex core velocity, (ms^{-1})
w	cross stream velocity, (ms^{-1})
x	length, (m)
α	angle of incidence, (deg)
Γ	circulation, (m^2s^{-1})
Ω	rotation velocity of rotor, ($rads^{-1}$)
ρ	freestream density, (kgm^{-3})
ν	kinematic viscosity, (m^2s^{-1})

1 Introduction

Blade vortex interactions (BVI) in rotorcraft are a well-known source of unwanted noise and vibration. They are caused when the trailing vortex from a main rotor blade encounters another blade on the aircraft. Much research has been performed for the case of main rotor BVI where the vortex interacts with another main rotor blade [1,2]. Less is known about the interaction of the main rotor vortex system and the tail rotor. A number of practical acoustic studies concerning the helicopter tail rotor interaction can be found in the literature. Examples of these include in-flight and wind tunnel acoustics measurements [3,4] and numerical studies [5,6]. Other researchers found that noise levels could be lowered by reduction of the tail rotor tip velocity [7] or reversal of rotation direction [8] or both [9]. An in-flight study by Ellin [10] considered the degradation in control produced by the tail rotor vortex interaction. These studies highlight the importance of the tail rotor vortex interaction for helicopter operation and design, however they leave

the details of the specific fluid dynamic mechanisms unresolved.

During tail rotor BVI, the main rotor vortex is ingested into the tail rotor disk. In this case, if the thickness of the leading edge of the tail rotor blade is sufficiently small, the vortex is severed or cut as it collides with the blade. It should also be pointed out that similar blade vortex interactions may occur in the compressor cascades of turbomachinery [11]. The trailing vortex can approach the tail rotor blades at various angles at different flight conditions. A limiting case of the tail rotor vortex interaction is where the vortex approaches a tail rotor blade orthogonally (Fig. 1).

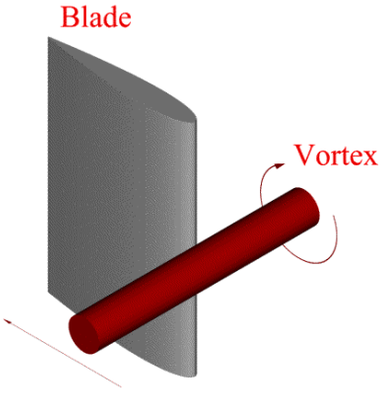

Fig.1 Illustration of the orthogonal Blade Vortex Interaction

Previous research into the basic orthogonal vortex interaction has included mathematical and experimental studies. Analytical investigations have been performed by Marshall [12]. Computational investigations using different numerical approaches [13,14,15] show that the vortex dynamics during cutting are controlled by the axial flow within the vortex core. If the axial flow is directed toward the cutting surface, the core bulges and if the axial flow is away from the surface, the core thins. Flow visualisations of the vortex cutting process [15,16,17] verify the core bulging and thinning and also show the production of secondary vorticity and entrainment of the blade boundary layer into the core. Surface pressure and noise measurements of the orthogonal vortex interaction [18,19] show a difference in pressure measurements on either side of the cutting surface which could possibly be due to an axial core component. Although these studies are important, it is difficult to resolve the instantaneous surface pressures over the entire chord during vortex cutting in the published data. Also, the experimental apparatus in the previous research produce vortices which are representative of the wake of a hovering rotor or propeller rather than a helicopter in forward flight.

The importance of generating the correct vortex geometry should not be underestimated. When data pertaining to blade vortex interactions are acquired from experiments in which the generation of the interacting vortex differs, there are clear differences in the flow development. How important these differences are is not clear, and it may be that they simply affect the peripheral response and not the fundamental interaction. Nonetheless, whatever system is used, it is essential that the detailed structure of the interacting vortex is known. It is also important to have a good knowledge of the vortex trajectory, stability and tendency to wander from its mean path. This applies irrespective of the method of generation. To mimic the convection of a main rotor tip vortex requires the generation of a transverse vortex that will travel in a stable fashion through the wind tunnel's working section. In the present study this was achieved using a single bladed rotor placed in the settling chamber of a wind tunnel [20]. The tip vortex system produced by this rotor exhibited the same characteristic features as a helicopter main rotor and so provided the basis for interaction studies. To confirm this, velocity measurements of the three-dimensional vortex were obtained using hot wire anemometry and particle image velocimetry.

In the present paper, detailed results from an extensive series of experiments investigating the orthogonal vortex interaction are presented. In all cases the results are for a vortex interacting with a stationary blade that was positioned downstream of the vortex generator in the wind tunnel working section. Firstly, chordwise pressures [21] and flow visualisation data [22] for the basic orthogonal interaction of the vortex with an unloaded blade are presented. The effect of vortex onset angle is then briefly introduced before a detailed examination of the effect of blade incidence [23] is presented. Also, the severity of a secondary interaction is considered by pre-cutting the vortex prior to interaction with the instrumented blade [24]. Finally, the remaining stages of the test programme will be outlined.

2 Methods

The experiments were conducted in the Glasgow University 1.15m x 0.85m low speed wind tunnel. This is a closed return facility with a working section length of 1.8m and is capable of speeds up to 33ms^{-1}. During testing, the free-stream velocity and temperature were monitored continuously using a pitot-static tube and thermocouple device located in the working section. The design of the vortex generator has been previously detailed by Copland [20] but will, for convenience, be summarised here. The vortex generator is essentially a rotor of radius 0.75m that has a single rectangular planform blade of chord 0.1m with a NACA 0015 cross section. During rotation, the blade pitch is varied using a spring-loaded pitch link running on a cylindrical cam configured such that the blade pitch varies in four equivalent (90^o) phases of azimuth. The first phase sets the blade at zero incidence while the blade is pointing into the settling chamber (45^o azimuthal travel on either side of the wind tunnel centre line). In the next two phases of motion, the blade is pitched from zero to 10^o, before traversing the working section at a constant 10^o incidence. In the final 90^o phase, the spring loaded pitch link forces the blade to overcome its aerodynamic and inertial loads and follow the cam as it returns to zero degrees.

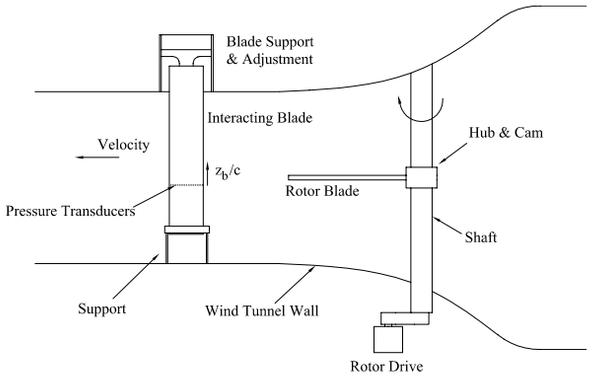

Fig. 2 Test set-up

The rotor assembly is mounted on a vertical rotating shaft that is supported by bearings which are installed in an external framework above and below the wind tunnel contraction. Also located on this framework is a DC electric motor that is used to drive the rig. During operation the rotational speed is monitored by an optical sensor located on the main shaft. Velocity measurements of the convecting vortex were made using a TSI IFA-300 Hot Wire Anemometer system using DANTEC 55P61 cross wire probes. The probes used 5mm diameter platinum plated tungsten wires with a length-to-diameter ratio of 250. The measuring volume of the probe was approximately 0.8mm in diameter and 0.5mm in height. The probe was calibrated in a special wind tunnel dedicated to the purpose. During calibration, the probe was rotated (in 6^o steps) ±30^o in the plane of the sensor wires to determine yaw sensitivity. A full account of the calibration procedures used can be found in Copland [20]. Data were recorded at 10kHz in 2048 sample blocks.

Independent velocity measurements were also made using a particle image velocimetry (PIV) system based on a Spectra-Physics Nd:Yag laser. By operating the laser in a double-pulsed mode, two images of the flow field can be obtained with very small time separation (50μs). A standard cross-correlation and sub-pixel peak detection routine can then be used to determine the mean velocity at various locations in the region of interest. In this work, two PIV systems were used to obtain separate flow field results of the same vortex but at different locations along the chord. The system uses two lasers and two cameras carefully timed to give results separated in time. The flow was seeded with 1-2μm oil smoke particles distributed throughout the flow. The laser light was passed through an optical arrangement which converted the beam into a laser sheet which was passed through the working section and illuminated the flow seeding. The particle displacements could then be recorded using two Kodak Megaplus ES 1.0 cameras of 1k x 1k resolution. The experiment was designed so that each camera detected the flow pattern illuminated by its own laser. Full details of the PIV technique used in this study are presented in Ref 22.

The vortex generator produces a curved, three-dimensional vortex that convects through the wind tunnel working section. A NACA 0015 blade of chord 152.4mm and overall span 944mm was placed in the path of the convecting vortex in order to study the interaction of the vortex with the blade. The experimental setup allowed a variation of the geometric incidence of the blade. Measurements were obtained within a blade incidence range of ±10^o using 2^o increments. When set at 0^o, the leading edge of the blade was 2000mm or 13.12 blade chord lengths downstream of the rotor centre line. The blade was

instrumented at 78.5% span with a chordal array of 30 miniature Kulite pressure transducers mounted around the surface of the blade. The transducers were connected to a surface orifice of 1mm diameter. For all tests the freestream velocity was fixed at 20ms^{-1} and the rotational speed of the vortex generator was 500 RPM. These settings had been previously identified by Doolan et al. [25] to provide a clear, well defined tip vortex structure in the working section. Based on these conditions, the nominal interacting blade Reynold's number was 2x10^5. As shown schematically in Fig. 2, the blade was mounted from the roof of the working section and extended to the tunnel floor. To facilitate the change in incidence of the blade, a specially designed support was located on the tunnel floor. Also, the blade was placed in two positions, each 225mm from the tunnel centreline (Fig. 3) in order to avoid the turbulent wake of the vortex generator support shaft. Previous velocity measurements have shown that the vortex is obscured by this wake [25].

To study secondary interactions another blade of identical chord and profile was installed one chord length upstream of the instrumented blade. The upstream blade contained no instrumentation and was used to simulate the effects of a preceding blade in a helicopter tail rotor.

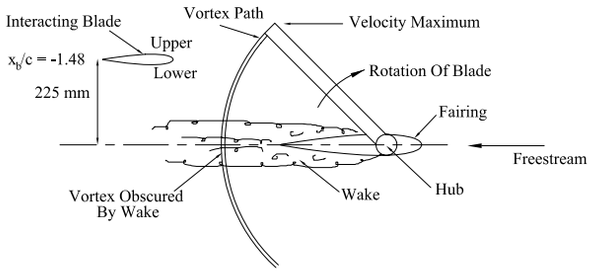

Fig. 3 Plan view of set-up showing blade position

Pressure data for each transducer were recorded using a BE256 data logger in a single 32000 sample block at 20kHz sampling rate. This sample rate and size allowed approximately 13 rotor revolutions of data capture. Five blocks of data were obtained at each blade incidence.

3 Results and Discussion

3.1 Vortex Velocity Measurements

The approach angle between the convecting vortex and instrumented blade was calculated using a free wake model of the trailing vortex and a source panel representation of the wind tunnel walls [26]. Hot-wire measurements were then used to verify the free-wake model results. This was done by taking simultaneous cross and single wire probe measurements at various lateral separation distances. Setting the vertical height of the probe outside of the interaction region, the measured time difference between the vortex passing each probe is a direct measurement of relative wake position. These measurements were compared with a two-dimensional projection of the computed wake structure at an equivalent time, which is shown in Fig.4. Very good agreement is observed, suggesting that the coupled panel method and free wake model provides a good representation of the wake geometry in the wind tunnel.

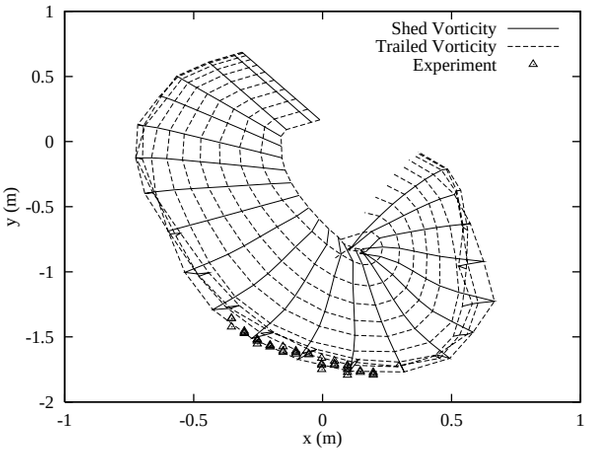

Fig. 4 Comparison of computed wake geometry with hot-wire measurements

Hot wire velocity measurements were taken at the position of the instrumented blade leading edge prior to the installation of the blade. During the test, the probe was traversed vertically through the working section and the transient vortex velocity field was acquired. The height of vortex core passage was considered to be the position where, on average, the maximum vertical velocity signal (v) was recorded (it is directly related to the vortex tangential velocity,

through a simple transformation [25]). The blade was then installed so the transducers were placed at this height and therefore in the path of the vortex core. A typical hot-wire vertical velocity record is shown in Fig. 5. Some variation between successive vortices was observed due to vortex wandering and local turbulence levels.

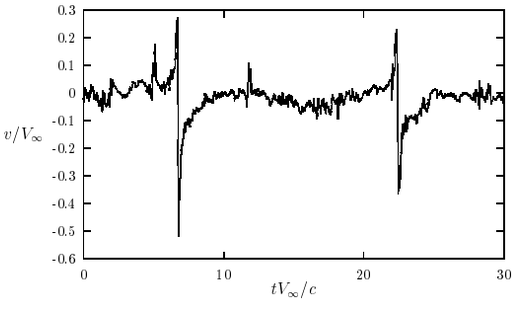

Fig. 5 Typical vertical velocity trace through vortex core

Particle image velocimetry (PIV) was also used to verify the position of the vortex and to quantify the total circulation about the core. A relatively high rotational velocity gradient exists within the vortex core which subjects entrained smoke particles to high centripetal and coriolis accelerations. Any particles initially within the core follow a spiral path which ejects them into the surrounding fluid. This was noticed as a dramatic drop in seed particle density within the vortex core region and hence the PIV system has poor resolution of the velocities within the core. The PIV measurements are therefore more useful for measuring the total circulation of the vortex rather than information within the core. Errors induced in the circulation measurements by vortex wandering in probe-based techniques can be reduced using PIV if the sampling region is larger than the wandering amplitude of the vortex. A summary of the vortex parameters measured using both PIV and Hot-wire anemometry can be found in Table 1. The hot wire results were used to obtain estimates of the vortex core size. This is defined as the distance between the peak tangential velocities on a line passing through the vortex centre. The PIV measurements were used to obtain the vortex circulation. The hot wire measurements were also used to obtain circulation measurements and the differences are indicated on the table. The benefits of using the PIV system are obvious with the uncertainty in the measurements reduced by 50%.

r_c/c	0.065±0.031
$\Gamma/\ \Omega R\ c_R$ (PIV)	0.144±0.022
$\Gamma/\ \Omega R\ c_R$ (Hot wire)	0.120±0.044
W/V_∞	0.4±0.12

Table 1: A summary of vortex parameters.

The vortex information presented above was used to estimate the blade impact parameter ($2\pi r_c V_\infty/\Gamma$ = 2.16). This has been identified by Marshall and Krisnamoorthy [15] as a quantity which indicates the severity of the physical response to the vortex cut. The value of the blade impact parameter obtained here implies that a weak interaction occurs during the experiments with no boundary layer separation before the vortex collides with the leading edge. It has been shown by Krisnamoorthy and Marshall [16] that the weak vortex interaction is the dominant tail rotor interaction mechanism for a helicopter in forward flight with an advance ratio greater than approximately 0.1.

The last row of Table 1 is indicative of a significant cross-stream velocity associated with the vortex core axial flow. When the model is installed in the wind tunnel, the direction of the core flow is towards the lower surface and away from the upper surface. The value of the axial flow parameter ($2\pi r_c W/\Gamma$ = 0.89) determines some aspects of the vortex dynamics during a vortex cut. For these experiments the value reported above indicates that the vortex is supercritical and only downstream area-waves of small amplitude can be supported on the vortex core [15]. If the vortex is supercritical it can be expected that when the vortex impacts with the instrumented blade, a jet-like flow will occur on the lower surface and a thinning of the vortex core will occur on the upper surface.

3.2 Basic Orthogonal Interaction

3.2.1 Pressure measurements

For the basic orthogonal interaction tests, the interacting blade was placed 225mm to the right of the

wind tunnel working section centreline. It was known, from the results of the numerical model and the hot-wire measurements, that the vortex approached this location at 90^o to the mean flow direction. The unsteady blade pressures were converted to pressure coefficients using the recorded freestream velocity, air density and pressure. When interpreting the results presented below, it should also be noted here that the upper surface experiences a vortex core flow away from the surface while the lower surface experiences a core flow directed toward the surface.

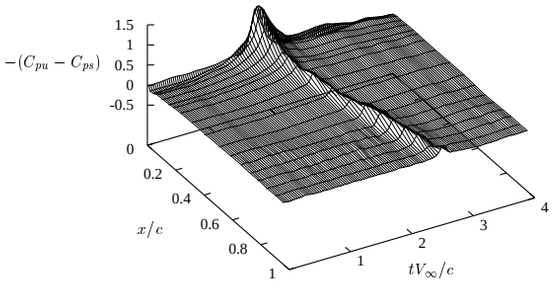

Fig. 6a Unsteady upper surface pressures during a clean orthogonal interaction

Figure 6 illustrates the temporal variation of the pressure data recorded as the vortex was cut by the blade when the transducers were placed in the path of the core. In each plot, the steady component of the pressure signal has been removed in order to increase the clarity of the results. The steady component was determined by averaging 32000 pressure samples obtained while the rotor rig was idle and making sure the interacting blade was not in the rotor blade wake. Hence, -(Cp_u-Cp_s) is plotted on the vertical axis with the chord position of the transducers (x/c) on one axis and non-dimensional time (tV/c) on the axis in the foreground. To further increase the clarity of the plots only every fifth data sample is presented. The upper surface interaction data in Fig. 6a shows a strong suction peak at the leading edge when the vortex first encounters the blade. As the vortex passes over the surface, the suction peak diminishes, but is still significant over the remainder of the chord. For the lower surface (Fig. 6b), an increase in pressure occurs just downstream of the leading edge but is rapidly diminished as the vortex travels over the blade surface. At approximately the quarter chord point, the pressure ridge transforms into a slight suction ridge that continues to convect towards the trailing edge.

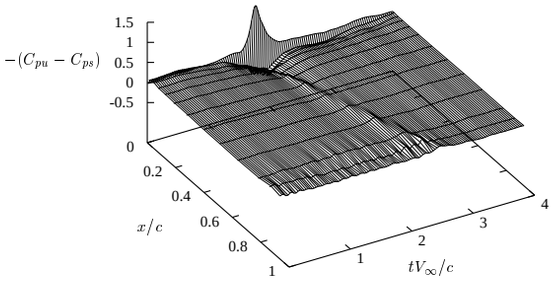

Fig. 6a Unsteady lower surface pressures during a clean orthogonal interaction

The surface pressure results obtained are interesting and illustrate the complexity of the vortex interaction. Although the only results presented here have been for the transducer array aligned with the vortex core, measurements were made, and have been fully documented [21], above and below the vortex core path. Common to all records is the presence of a suction peak on the upper and a pressure peak on the lower surface in the vicinity of the leading edge. This aerodynamic response can be explained in terms of the core axial flow. For the current configuration, the vortex axial flow is expected to travel towards the lower surface and away from the upper surface hence initiating the pressure and suction peaks observed. It is likely that after the initial vortex cut any axial core flow will be greatly reduced. After this has occurred, the low pressure within the vortex core would be allowed to dominate, thereby creating a suction ridge over the surface. This explanation is not without precedent, as flow visualisation studies of the vortex cut in a water tank [15] show that the boundary layer on both sides of the blade is entrained into the core after the initial cut, even with the presence of a strong core axial component. It should be noted that, in the lower surface plots, the leading edge pressure record is repeated for completeness.

3.2.2 Particle Image Velocimetry

The rotor and laser system were synchronised so that the laser pulses illuminated the vortex as it passed through the required location(s) in the wind tunnel.

By varying the delay between the two lasers and by moving the blade along the tunnel working section, the vortex interaction was investigated along the entire blade chord. The results presented here were obtained by placing the laser sheet 15mm from the blade centre-line, parallel to the blade chord. At the maximum blade thickness the laser sheet was at a distance of only 3mm from the lower blade surface.

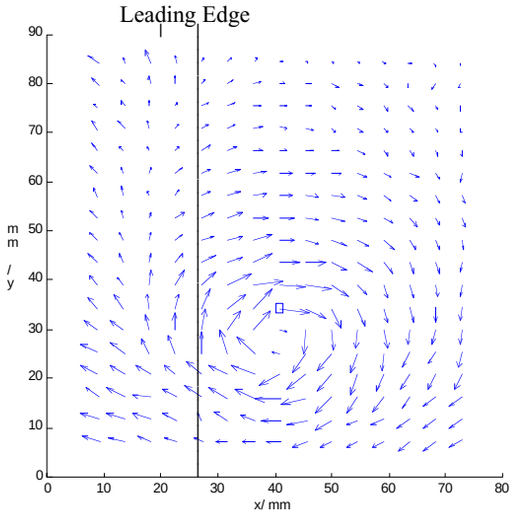

Fig. 7a Vortex approaching leading edge

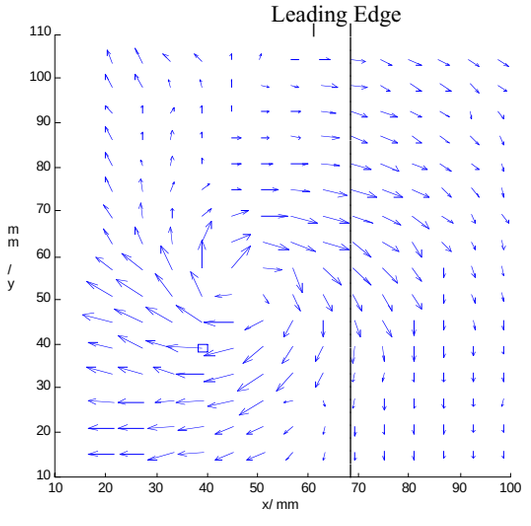

Fig. 7b Vortex crossing leading edge

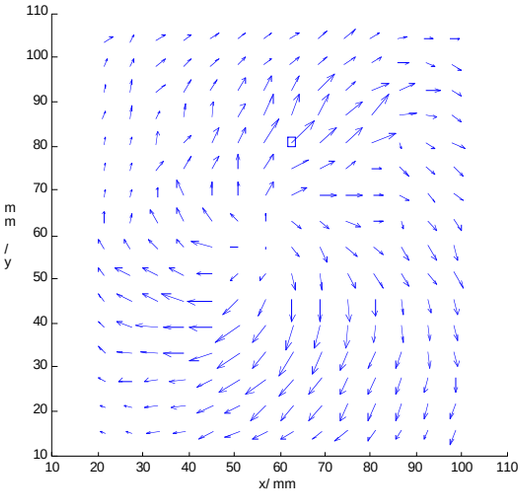

Fig. 7c Vortex just past mid-chord

Figure 7 shows the vortex flow field as the vortex collides with the leading edge. In each frame, the leading edge is indicated and the mean horizontal velocity component has been removed in order to highlight the vortex flow. In Fig. 7a the vortex is just upstream of the leading edge. Figure 7b shows the same vortex 1.7ms later, after it has interacted with the leading edge. The velocity vectors in Fig. 7b suggest that the velocity vectors are spiralling outwards from the vortex core. This effect can be seen more clearly in Fig. 7c which shows the vortex at a location further downstream. The production of the source-like outflow after blade-vortex interaction is thought to originate from the vortex core axial flow. Axial core flow is expected to flow toward the blade during these tests. Hence, as the vortex passes over the blade, the blade surface will block the core flow and direct it radially over the blade surface. This is in general agreement with previously published computational results which show the core flow dispersing radially during an instantaneous vortex cut. The radial flow significantly alters the vorticity distribution of the vortex. The source flow effectively enlarges the vortex and generally decreases vorticity levels.

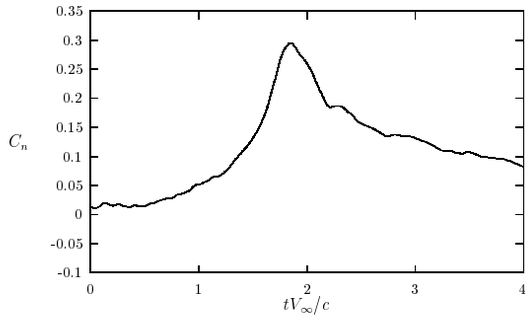

Fig. 8a Normal force coefficient during clean orthogonal interaction

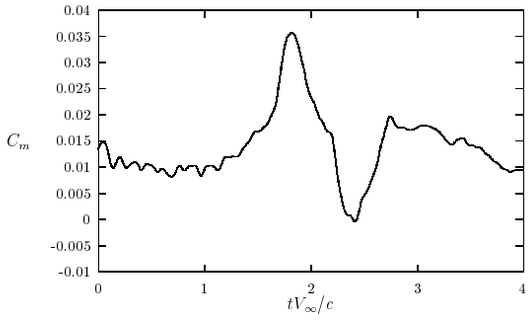

Fig. 8b Pitching moment coefficient during clean orthogonal interaction

3.2.3 Force and Pitching Moment Data

The pressure data were integrated over the blade surface to give normal force and quarter chord pitching moment coefficients during the vortex interaction. Figure 8 plots the force and moment coefficient data against non-dimensionalised time for the transducer array aligned with the vortex core. A significant, impulsive normal force is experienced by the blade (Fig. 8a) as the vortex is cut by the leading edge. The normal force then decays as the vortex travels down the chord. The quarter chord pitching moment data (Fig. 8b) illustrates a large nose up moment is experienced by the blade as the vortex approaches the leading edge. A rapid change in pitching moment sign is subsequently observed which can be attributed to vortex passing the quarter chord point. Finally, pre-interaction pitching moment values are recovered after the vortex passes over the trailing edge.

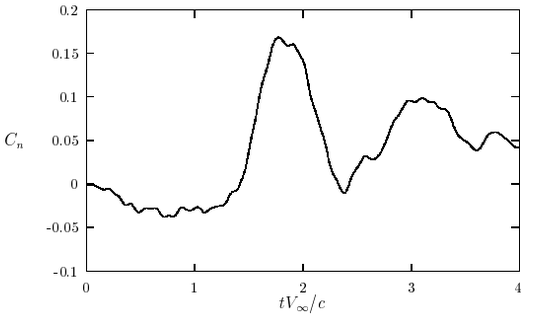

Fig. 9a Normal force coefficient during non-orthogonal interaction

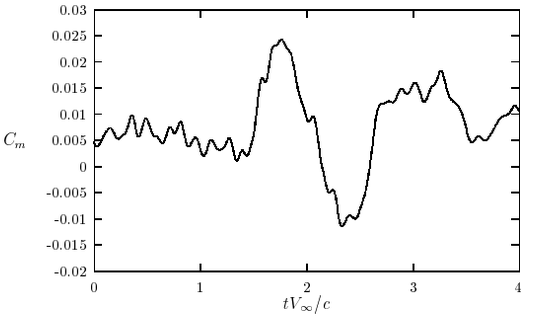

Fig. 9b Pitching moment coefficient during non-orthogonal interaction

3.3 Effect of Vortex Approach Angle

The effect of a significant change in vortex approach angle was studied by placing the interacting blade 225mm to the left of the wind tunnel centreline. At this location, both the hot-wire measurements and the numerical model indicated that the vortex approach angle was approximately 42°. The general characteristics of the pressure response for this case were similar to those of the purely orthogonal case although the magnitude of the response is not as great. In addition, some specific differences were observed. In particular, the suction ridge over the trailing edge on the upper surface was not as sharp and there was no establishment of a suction ridge on the lower surface. These general observations are manifest in the normal force and pitching moment coefficient results presented in Fig. 9 where it may be observed that the both the normal force and pitching moment responses are reduced in comparison with the orthogonal case.

3.4 Effect of Blade Incidence

The general form of the pressure response during interaction with a loaded blade is very similar in form to the zero incidence case. The main difference, at moderate incidence, is the magnitude of the suction and pressure peaks achieved. The measurements show that the suction peak on the upper surface leading edge is seen to intensify when the blade is set at positive incidence and reduce somewhat at negative incidence. This effect can be observed in more detail in Fig. 10a where peak suction measurements obtained during the interaction from a transducer placed at x/c = 0.009 are plotted against blade incidence. Each data point represents an average of twenty interactions and the error bars indicate one standard deviation either side of the mean. Despite a significant scatter, thought to be due to vortex wandering, the results show the suction peak increases in magnitude on the upper surface as the blade incidence is increased. Further, a clear maximum is observed at $\alpha = 6^o$. This maximum in suction peak also occurs at the same incidence setting for transducer locations further downstream. With the blade incidence set below $\alpha = -4^o$, the mean value in suction peak is reduced (compared with $\alpha = 0^o$) and remains relatively constant.

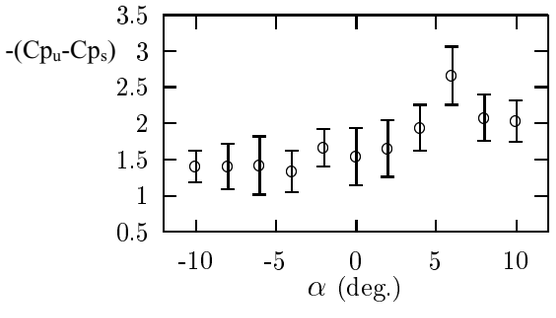

Fig. 10a Upper surface leading edge peak suction versus incidence

On the lower surface, the change in incidence has a similar effect on the observed pressure pulse. As the incidence is increased in the positive sense the pressure pulse is reduced. When the incidence becomes negative the pressure pulse at the leading edge increases in magnitude. In Fig. 10b, the peak pressure results from twenty orthogonal vortex interactions have been extracted from a transducer on the lower surface and near the leading edge (x/c = 0.011). An increase in pressure pulse magnitude (denoted by a decrease in $(Cp_u\text{-}Cp_s)$) with decreasing incidence can be observed from the results. The general form of the curve is monotonic except at negative incidence values beyond $\alpha = -5^o$. It is interesting to note that, in this respect, this behaviour is almost a mirror image of that presented in Fig. 10a.

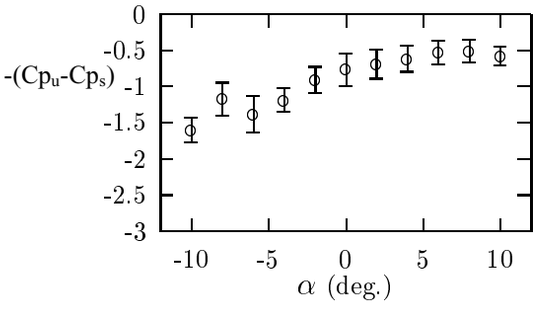

Fig. 10b Lower surface leading edge peak suction versus incidence

The way in which the above changes are manifest in the normal force response is particularly interesting. Figure 11 shows the variation in the difference between the peak and time averaged normal force coefficients during the interaction over the range of incidence settings used in the experiments. The plotted value ΔCn therefore represents the impulsive normal load imparted to the blade by the interaction of the vortex only with the offset of the steady aerodynamics removed. Each data point in Fig. 11 represents the mean of twenty vortex interactions and the error-bars indicate the standard deviation. The results show that as the blade incidence is changed, the impulsive peak normal force experienced by the blade is approximately the same. It is worth noting that recent normal force measurements taken during a simulated main rotor blade vortex interaction [2] indicate a similar result despite the fact that the vortex interaction is of a different type.

It would appear that the peak magnitude in normal force is maintained due to the amplification and attenuation of suction and pressure peaks around the leading edge at different incidence settings. At positive incidence, the suction peak is increased while the pressure pulse is reduced and the opposite is true at negative incidence. Therefore, even if the upper and lower surface pressure distributions are altered, the overall effect on transient normal force is the same.

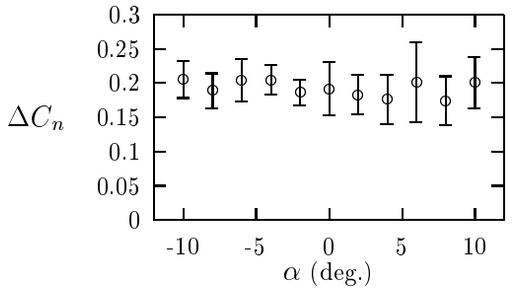

Fig. 11 Variation of impulsive normal force with incidence

3.5 Effect of Blade Pre-Cut

In forward flight, the main rotor tip vortex may be cut several times by tail rotor blades after the initial interaction. The extent to which these secondary interactions are significant in terms of noise generation is presently unknown. In an attempt to gain a basic insight into this phenomenon, a series of experiments were conducted in which the vortex was pre-cut by a blade located one chord length upstream of the instrumented blade. The results of this study have been fully reported in Ref. 24 but are summarised here.

Surface pressure measurements of the vortex interaction which occurs when an upstream or preceding blade is installed are shown in Fig. 12. The results are of generally the same nature as the clean interaction tests but are reduced in magnitude. A suction ridge develops on the upper surface and a mild pressure pulse transforms into a very weak suction ridge on the lower surface in a similar way to the clean interaction tests.

The similarity between these results and the clean interaction data indicates that a complete vortex exists before the interaction with the instrumented blade. As the vortex is completely severed by the first interaction, the vortex must reconnect within the space between the two blades. The extent of the similarity suggests that the reconnection process is complete with both rotational and axial velocity components being re-established. Vortex reconnection after an orthogonal interaction has been visualised previously by Johnston and Sullivan[19] however it was uncertain whether the axial component was destroyed. The results presented here indicate that while the vortex cutting process removes significant momentum from the core, complete destruction is avoided. As the vortex strength is expected to increase away from the blade, a pressure gradient will exist along the core which may promote the regeneration of both the axial and rotational flow components.

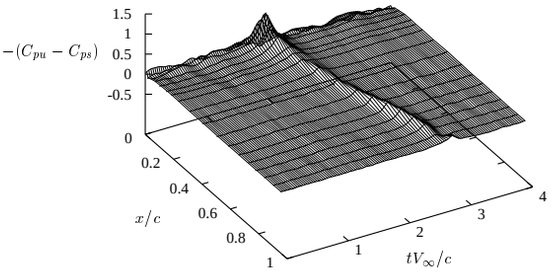

Fig. 12a Unsteady upper surface pressures during a secondary interaction

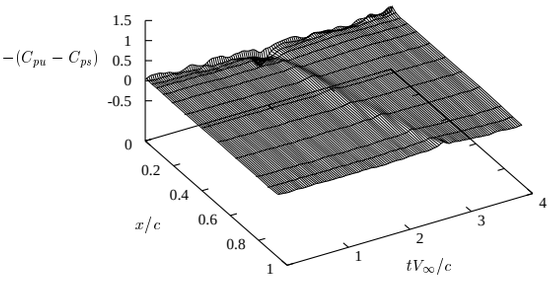

Fig. 12b Unsteady lower surface pressures during a secondary interaction

It is worthy of note that, with a preceding blade installed, the transient surface pressure recorded at the leading edge transducer does not show the strong suction peak recorded for the clean interaction tests. In fact, the presence of a suction peak at the leading edge transducer is somewhat intermittent between interactions when a preceding blade is installed. The leading edge suction represents the low pressure within the vortex core. As the vortex is in the process of reconnection it is possible that successive vortices are in different stages of reform, hence with different pressure levels within the core. From the results presented here, further study of the vortex

reconnection process is required to achieve a more complete understanding of this event.

As may be expected from the pressure data, the normal force and pitching moment coefficient curves exhibit the same basic features as those of the clean interaction case. The most significant difference is the a reduction in the severity of the response to the interaction.

4 Current and Future Work

A two-stage test programme is currently under way to provide further insight into the interaction phenomenon. The first stage of the work, which has just been completed, involves the measurement of vortex interactions on a stationary blade in the same manner as before but in a much larger test facility. The wind tunnel being used has working section dimensions 2.65m x 2.04m and tests are being conducted at wind speeds up to 50m/s. Figure 13 shows the vortex generator installed in the wind tunnel prior to the addition of aerodynamic fairings. The interacting blade is, this time, instrumented with around ninety miniature pressure transducers in a manner such that the full three-dimensional nature of the interaction can be measured. The blade, which is mounted vertically in the wind tunnel, can be moved up or down to vary the location of the transducers in relation to the vortex core. It has been found that the vortex position is much more stable in the current test series and so it is anticipated that by moving the blade in this way a very detailed three-dimensional picture of the interaction process will be obtained.

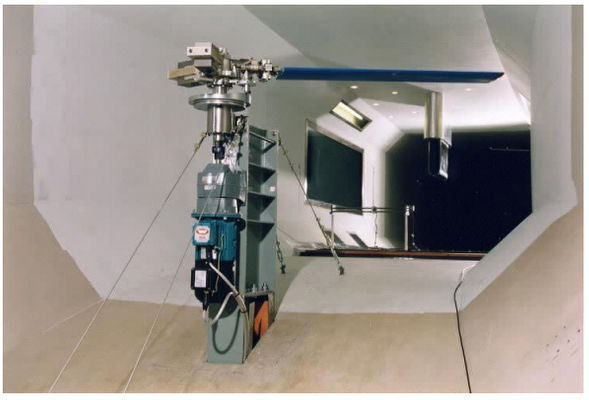

Fig. 13 Vortex generator in 2.65m x 2.04m wind tunnel

In the second stage of the programme, the stationary blade will be replaced by a model tail rotor. This rotor will have a limited number of pressure transducers installed on each blade and it is hoped that both primary and secondary interactions can be detected. In addition, it should be possible to identify the extent to which the interaction is modified as a result of the tail rotor inflow.

5 Concluding Remarks

The interaction of a three-dimensional rotor tip vortex with a symmetrical blade has been investigated using unsteady pressure measurement and PIV. The tests have encompassed the basic orthogonal interaction on an unloaded blade and a range of variants including interaction with a blade at incidence, non-orthogonal interaction and secondary interaction. In all cases, the response during the interaction is dominated by the axial core flow within the vortex. This is even the case during the secondary interaction when the vortex has been pre-cut, suggesting that vortex reformation takes place shortly after a BVI event.

Work is continuing in this area and it is hoped that a test programme currently under way will provide more insight into the three-dimensionality of the problem and the extent to which interactions are modified by the actual tail rotor environment.

Acknowledgements

This work was funded by the Engineering and Physical Sciences Reseach Council (EPSRC), the British Ministry of Defence (MOD), the Defence Evaluation and Research Agency, Farnborough and GKN-Westland Helicopters Ltd under grant number GR/L 58231 through the EPSRC/MOD joint grants scheme.

References

1. Straus, J., Renzoni, P., and Mayle, R., ``Airfoil Pressure Measurements during a Blade-Vortex Interaction and Comparison with Theory,'' *AIAA Journal* , Vol. 28, 1990, pp.222-228.

2. Masson, C., Green, R., Galbraith, R., and Coton, F., ``Experimental Investigation of a Loaded Rotor Blade's Interaction with a single vortex," *The*

Aeronautical Journal , Vol. 102, No. 1018, 1998, pp. 451-457.
3. Samokhin, V.F. Impulsive noise of the helicopter tail rotor, 21st European Helicopter Forum, St-Petersberg, Russia, Aug-Sept, 1995.
4. Schultz, K.J. and Splettstoesser, W.R. Helicopter main rotor/tail rotor noise radiation characteristics from scaled model rotor experiments in the DNW, 49th Annual Forum of the American Helicopter Society, St-Louis, USA, May 1993.
5. Howe, M.S. On unsteady surface forces and sound produced by the normal chopping of a rectilinear vortex, *J Fluid Mech*, 1989, 206, pp 131-153.
6. George, A.R. and Chou, S.T. Helicopter tail rotor blade-vortex interaction noise, NASA Contractor Report 183178, March 1987.
7. Jacobs E.W., Mancini, J., Visintainer, J.A. and Jackson, T.A. Acoustic flight test results for the Sikorsky S-76 quiet tail rotor at reduced tip speed, 53rd Annual Forum of the American helicopter Society, Virginia Beach, USA, April-May 1997.
8. Leverton, J.W., Pollard, J.S. and Wills, C.R. Main rotor wake/tail rotor interaction, *Vertica*, 1977, 1, pp 213-221.
9. Leverton, J.W. and Pike, T.C. The importance of tail rotor interaction as an acoustic source, 49th Annual Forum of the American Helicopter Society, St-Louis, USA, May 1993.
10. Ellin, A.D.S. An in flight Study of Lynx AH MK5 main rotor/tail rotor interactions, 19th European Helicopter Forum, Cernobbio, Italy, September, 1993.
11. Conlisk, A., ``A Theory of Vortex-Surface Collisions," AIAA Paper No: 98-2858 , June 1998.
12. Marshall, J., ``Vortex Cutting by a Blade, Part 1: General Theory and a Simple Solution," *AIAA Journal* , Vol. 32, No. 6, 1994, pp. 1145-1150.
13. Marshall, J. and Yalamanchili, R., ``Vortex Cutting by a Blade, Part 2: Computations of Vortex Response," *AIAA Journal* , Vol. 32, No. 7, 1994, pp. 1428-1436.
14. Lee, J., Burggraf, O., and Conlisk, A., ``On the Impulsive Blocking of a Vortex Jet,'' *Journal of Fluid Mechanics* , Vol. 369, 1998, pp. 301-331.
15. Marshall, J. and Krishnamoorthy, S., ``On the Instantaneous Cutting of a Columnar Vortex with Non-Zero Axial Flow," *Journal of Fluid Mechanics* , Vol. 351, 1997, pp. 41-74.
16. Krishnamoorthy, S. and Marshall, J., ``Three-Dimensional Blade Vortex Interaction in the Strong Vortex Regime," *Physics of Fluids* , Vol. 10, No. 11, 1998, pp. 2828-2845.
17. Cary, C., ``An Experimental Investigation of the Chopping of Helicopter Main Rotor Tip Vorticies by the Tail Rotor. Part II: High Speed Photographic Study," Contractor Report 177457, NASA, September 1987.
18. Ahmadi, A., ``An Experimental Investigation of Blade-Vortex Interaction at Normal Incidence,'' *AIAA Journal* , Vol. 23, No. 1, 1986, pp. 47-55.
19. Johnston, R. and Sullivan, J., ``Unsteady Wing Surface Pressures in the Wake of a Propeller," AIAA Paper No: 92-0277 , June 1998.
20. Copland, C., ``Methods of Generating Vortices in Wind Tunnels," Ph.D. thesis, Department of Aerospace Engineering, University of Glasgow, 1997.
21. Doolan, C., Coton, F., and Galbraith, R., ``Three-Dimensional Vortex Interactions with a Stationary Blade," *The Aeronautical Journal* , Vol. 103, No. 1030, 1999, pp. 579-587.
22. Green, R.B., Doolan, C.J., Cannon, R., 'Measurements of the orthogonal blade vortex interaction using a PIV technique', Accepted for publication in *Experiments in Fluids*
23. Doolan, C., Coton, F., and Galbraith, R.," Surface Pressure Measurements of the Orthogonal Vortex Interaction", Accepted for publication in the *AIAA Journal*
24. Doolan, C., Coton, F., and Galbraith, R.," The Effect of a Preceding Blade on the Orthogonal Vortex Interaction", 56th American Helicopter Society Forum, Virginia Beach, May 2000
25. Doolan, C., Coton, F., and Galbraith, R., ``Measurement of Three-Dimensional Vortices using a Hot Wire Anemometer," AIAA Paper No: 99-3810 , June/July 1999.
26. Copland, C., Coton, F.N., Galbraith, R.A.McD., 'A study of helicopter tail rotor interaction; Phase 1 – proof of concept', 24th European Rotorcraft Forum, Marseilles, France, 1998